Synaptopodin is required for long-term depression at Schaffer collateral-CA1 synapses

Yanis Inglebert[1,2*], Pei You Wu[1], Julia Tourbina-Kolomiets[1], Cong Loc Dang[1], R. Anne McKinney[1*]

[1] Department of Pharmacology and Therapeutics, McGill University, Montreal, Canada

[2] Current address Department of Neurosciences, Montreal University, Montreal, Canada

*Corresponding authors: anne.mckinney@mcgill.ca and yanis.inglebert@umontreal.ca

Keywords: Synaptopodin, synaptic plasticity, hippocampus, STDP, LTD, IP3

4343 words, 18 pages, 36 references, 4 figures

Abstract

Synaptopodin (SP), an actin-associated protein found in telencephalic neurons, affects synaptic and structural plasticity. While being required for long-term depression (LTD) mediated by metabotropic glutamate receptor (mGluR-LTD), little is known about its role in other forms of LTD induced by low frequency stimulation (LFS-LTD) or spike-timing dependent plasticity (STDP). Using SP-deficient mice (SPKO), we have here demonstrated that the presence of SP is mandatory for normal LTD expression. On the contrary, long-term potentiation (LTP), albeit diminished in SPKO, is still present and can be easily recovered by increasing the stimulation frequency. Our study shows, for the first time, the role of SP in a more physiological form of induction of synaptic plasticity.

Introduction

Synaptopodin (SP) is a postsynaptic actin-associated protein found in a subset of mature dendritic spines [1]. Mainly found in the hippocampus and cortex, it is known to be involved in synaptic plasticity and spine remodeling [2,3]. For example, lack of SP has been shown to result in a reduced long-term potentiation (LTP) and deficits in spatial learning [4]. More recently, our group has demonstrated that SP is required for a form of long-term depression (LTD) mediated by group I metabotropic glutamate receptor (mGluR-LTD) [5,6]. However, it is unclear whether SP is also required for other forms of LTD. Additionally, two distinct forms of

plasticity induction based on synaptic activity coexist: Bienenstock-Cooper-Munroe (BCM) model and Spike-Timing Dependent Plasticity.

The first is a theoretical framework describing how synaptic plasticity can be modulated by the level of neuronal activity and the history of synaptic inputs [7]. In this paradigm, low-frequency stimulation (2 – 5 Hz) induces LTD (LFS-LTD) while high-frequency stimulation (10 – 100 Hz) induces LTP (HFS-LTP) but the threshold between LTD/LTP can be dynamically adjusted. Both require an increase in intracellular calcium (Ca^{2+}) from NMDA receptors (NMDAR), at least at CA3-CA1 synapses [8]. The role of SP in this form is still poorly understood. While some studies suggested that only spines containing SP are more likely to develop LFS-LTD [9], others reported a normal LFS-LTD in SP-deficient mice [10].

The second model is called Spike-Timing Dependent Plasticity (STDP). More physiological, rather than being dependent on the stimulation frequency, synaptic modifications are based on the precise timing between presynaptic (in the form of excitatory postsynaptic potential or EPSP) and postsynaptic (in the form of an action potential or AP) activity. These paradigms are thought to better mimic what happens in the brain [11]. Classically, timing-dependent long-term potentiation (t-LTP) is induced when an EPSP is followed by an AP in the postsynaptic neuron [12,13]. In contrast, timing-dependent long-term depression (t-LTD) is induced when an EPSP is preceded by an AP [14–16]. At CA3-CA1 synapses, both induction protocols also require intracellular calcium elevation, but while t-LTP requires strong Ca^{2+} entry from NMDA- and AMPA-receptors (AMPAR) activation, t-LTD relies on moderate Ca^{2+} release from internal stores through IP3 receptors (IP3R)

triggered by mGluR5 activation [17,18]. This is a general learning rule underlying memory found *in vitro* and *in vivo* in a wide range of species [19] but to date no study has explored the role of SP in STDP.

In this study, to better understand the role of SP at Schaffer collateral-CA1 synapses (Sc-CA1), we induced LFS-LTD/HFS-LTP or t-LTD/t-LTP in wild-type (WT) and SP-deficient mice (SPKO). Our results show that in the absence of SP, it is impossible to induce LFS-LTD or t-LTD. Nevertheless, although affected, t-LTP can be recovered by boosting Ca^{2+} entry through specific activity patterns. These results provide novel insight into the role of SP in LTD and describe SP as a key molecular component to enable synaptic plasticity.

Results

Synaptopodin is required for LTD induced by low frequency stimulation.

First, we wanted to determine the consequences of the absence of SP on synaptic plasticity induced by low- or high-frequency stimulation to gain an overview of the BCM curve. The Schaffer collaterals were stimulated with 900 pulses at 2, 10 or 100 Hz (**Fig 1A**). LFS-LTD and HFS-LTP are known to be induced respectively by 2 and 100 Hz while 10 Hz is generally the threshold between LTD/LTP. In SPKO, no significant change in synaptic modification (field EPSP slope measured on the last 10 minutes of the recording) was observed after 2 Hz (100.3 ± 1,7 vs 81.4 ± 6.1, $p < 0.003$, Mann-Whitney) and 10 Hz (110.68 ± 7.8 vs 152.96 ± 11.1, $p < 0.03$, Mann-Whitney) stimulation compared to WT (**Fig 1C, D**). In contrast, WT exhibited a robust LFS-LTD and HFS-LTP respectively for

2 Hz and 10 Hz stimulation. At 100 Hz, SPKO revealed a modest HFS-LTP in comparison to the magnitude found in WT (**Fig 1E**; 117.9 ± 3.4 vs 140.1 ± 3.7, $p < 0.001$, Mann-Whitney). Overall, in SPKO, our data suggest that LFS-LTD is absent and HFS-LTP amplitude is decreased (**Fig 1B**). Interestingly, the threshold for synaptic changes appears to be higher in the absence of SP.

Spike-timing dependent plasticity is altered in absence of synaptopodin

We next examined the consequences of the lack of SP on synaptic plasticity induced at the Schaffer collateral-CA1 pyramidal cell synapses by STDP (**Fig 2A, Left**). Classically, t-LTP was induced by repeatedly pairing (100 times, 0.3 Hz) an EPSP followed briefly (between +5 and +50ms, positive pairing) by a postsynaptic action potential (AP) (**Fig 2A, Right**). No t-LTP is observed in SPKO at +10ms, a timing that generally shows the highest t-LTP amplitude in WT. (**Fig 2B**, 83.3 ± 8,6 vs 139.2 ± 7,1, $p < 0.001$, Mann-Whitney). Instead, a robust t-LTD is observed. Construction of STDP curves for several timings exhibited a single LTD window ranging from +10ms to +30ms in SPKO (**Fig 2C, Right**) while the conventional LTP window is observed in WT (**Fig 2C, Left**). For negative pairing (a postsynaptic AP followed by an EPSP) at -25ms, a timing that generally shows the highest t-LTD amplitude in WT , no plasticity is observed in SPKO (**Fig 2D**, 96.2 ± 3.7 vs 71.9 ± 7.7, $p < 0,05$, Mann-Whitney). Rather, no plasticity is observed. These data indicate that the STDP rule is severely impaired in the absence of SP and t-LTD is totally absent for negative pairings.

t-LTP but not t-LTD can be rescued in absence of synaptopodin

STDP induction rules are flexible and can be adapted by modulating intracellular Ca^{2+} influx [20–22]. For example, an easy way to boost intracellular Ca^{2+} influx is to increase the stimulation frequency which would lead to cross the synaptic threshold for t-LTD and t-LTP. Taking this into account we attempted to recover t-LTP and t-LTD deficits in SPKO by increasing the pairing frequency. At +10ms, increasing the pairing frequency from 0.3 to 5 Hz has been sufficient to significantly recover the t-LTP window (**Fig 3A**, 129.9 ± 10.3, $p < 0,05$, Mann-Whitney). On the other hand, increasing the pairing frequency did not significantly recover t-LTD window at -25ms neither at 5 Hz (101.6 ± 5.7) nor at 10 Hz (87.7 ± 3.7) compared to 0.3 Hz (**Fig 3B**). Similarly to the results obtained in **Fig1**, t-LTP, while affected, can still be induced but t-LTD remained totally absent. We concluded that t-LTP can be rescued in SPKO but not t-LTD.

AMPA and IP3-receptors expression is altered in SPKO

To better understand what could lead to these deficits of synaptic plasticity, we next examined the expression level of the key receptors involved in these two forms of synaptic plasticity. NMDA, AMPA and IP3-receptors are the main sources of calcium to induce synaptic changes. Their expression level was analyzed by Western blot from hippocampi lysates of WT and SPKO. We particularly investigated GluA1/GluA2 subunit of AMPARs and GluN2A/GluN2B subunit of NMDARs because they are the major subunits found in the hippocampus [23,24]. Significant decrease was observed for total expression of AMPA-receptor subunits GluA1 (1.07±0.04 vs 0.81±0.03, $p<0.01$, unpaired t-test) and GluA2 (1.05±0.03 vs

0.92±0.02, p=0.01, unpaired t-test) in SPKO compared to WT (**Fig 4A**). Similar results were found regarding the surface expression of GluA1 (**Fig 4B**, 0.50±0.04 vs 0.37±0.04, p<0.05, unpaired t-test) and GluA2 (**Fig 4C**, 0.46±0.04 vs 0.33±0.03, p<0.01, unpaired t-test). In contrast, no difference in expression was found for NMDA receptor subunits GluN2A (**Fig 4D Left**, 0.90±0.03 vs 0.89±0.04, p>0.05, unpaired t-test) and GluN2B (**Fig 4D Right**, 0.94±0.04 vs 1.01±0.01, p>0.05, unpaired t-test). Finally, IP3-receptors expression was found to be significantly decreased in SPKO (**Fig 4E**, 1.00±0.06 vs 0.78±0.05, p<0.05, unpaired t-test). Overall, IP3- and AMPA- receptors expression was found to be significantly reduced unlike NMDA receptors.

Discussion

LFS-LTD is absent in SPKO

Our results revealed an absence of LFS-LTD in SPKO compared to WT (**Fig 1**). Our findings contradict previously published findings [10] that LFS-LTD was not modulated by loss of SP. The experimental conditions are similar regarding the stimulation protocol (2Hz 1200 stimuli vs 2Hz 900 stimuli) and the age of mice (P14-P25). An attractive explanation for this difference could be that the LFS-LTD threshold is higher in SPKO. In fact, previous studies have shown a relationship between the number of stimuli and LTD amplitude [25]. Another possible explanation is that the extracellular calcium concentrations used are different. While we used a more physiological concentration of calcium (2mM), Zhang et al, employed a concentration of 2.5mM. Higher calcium concentrations could lead to overestimation of plasticity [21,26].

BCM curve is shifted in SPKO

In SPKO slices, our data showed that at 10 Hz, HFS-LTP was absent. 10 Hz is a particularly interesting frequency, as it is considered to be the threshold (θm) between LTD and LTP [7]. This threshold is dynamic and slidable and can serve as a homeostatic mechanism to keep synapses within a modifiable zone in response to perturbations in neuronal activity. Interestingly, lack of SP has been linked to a loss of GABAergic inhibition [27] and increased excitability [28]. To compensate for this increase in CA1 cell excitability, the sliding threshold could horizontally shift to the right as demonstrated in other brain regions [29]. Further studies are required to better understand the role of SP in homeostatic plasticity at CA3-CA1 synapses. One elegant recent paper identified SP as a molecular tag to promote input-specific synaptic plasticity [30].

t-LTP can be rescued but not t-LTD

At Sc-CA1 synapses, both t-LTP and t-LTD require post-synaptic calcium (Ca^{2+}) elevation [31,32] but from different sources. The magnitude of the Ca^{2+} signal determines the direction/polarity of plasticity [33]. Whereas t-LTP relies almost solely on Ca^{2+} entry via post-synaptic NMDA receptors (NMDAR), t-LTD required activation of mGluR5 and subsequent IP3R-mediated Ca^{2+} release from internal stores [17] and both are affected by the absence of SP. As we previously reported, mGluR5 function and expression is impaired [6]. Moreover, SP is known to regulate release of Ca^{2+} from internal stores [34] and our results indicate that IP3R expression is impaired. In other words, if t-LTD is absent and impossible to recover, it's certainly because the needed molecular machinery is not present in the absence

of SP. In contrast, t-LTP can simply be recovered by increasing the pairing frequency (from 0.3 to 5 Hz) and therefore the post-synaptic calcium entry. In addition to NMDAR, AMPA receptors mediated EPSPs provide local depolarization to boost NMDAR current [35,36]. A reduction of AMPAR expression could reduced NMDAR current for a given depolarization explaining the absence of t-LTP observed at 0.3 Hz. A stronger protocol (5 Hz) enables the potentiation threshold to be crossed because NMDAR expression is not affected in SPKO, and the calcium entry provided by NMDAR only is now sufficient. Additional calcium imaging experiments will be required to better understand the calcium dynamics at the level of the single spine-expressing SP.

Our results demonstrate for the first time the central role of SP in LTD, particularly induced by STDP. These findings encourage further exploration and dissection of the role of SP in plasticity at the scale of the single spine. It could be the key to understanding why dendritic spines are not all equal when it comes to plasticity.

Materials and Methods

Animals

All procedures were according to protocols approved by the guidelines of the Canadian Council on Animal Care and the McGill University Comparative Medicine and Animal Resources animal handling protocols 5057. C57Bl6 (WT) or SPKO mice were used as previously described [2,22]. Mice were fed *ad libitum* and housed

with a 12 h light/dark cycle. WT and SPKO male and female mice were used for experiments.

Electrophysiology

Hippocampal *ex vivo* slices were obtained from P14-P25 old WT or SPKO mice. Mice were deeply anesthetized with isoflurane and killed by decapitation. Slices (400 µm or 350 µm) were cut on a vibratome (Leica Microsystems, VT1200S) in a sucrose-based solution containing the following (in mM): 280 sucrose, 26 $NaHCO_3$, 10 glucose, 1.3 KCl, 1 $CaCl_2$, and 10 $MgCl_2$ and were transferred at 32°C in regular ACSF containing the following (in mM): 124 NaCl, 5 KCl, 1.25 NaH_2PO_4, 2 $MgSO_4$, 26 $NaHCO_3$, 2 $CaCl_2$, and 10 glucose saturated with 95% O_2/5% CO_2 (pH 7.3, 300 mOsm) for 15 min before resting at room temperature (RT) for 1 h in oxygenated (95% O_2/5% CO_2) ACSF. Recordings were obtained using a Axopatch 200B (Molecular Devices) amplifier and pClamp10.4 software. Data were sampled at 10 kHz, filtered at 3 kHz, and digitized by a Digidata 1440A (Molecular Devices). Field excitatory postsynaptic potentials (fEPSPs) or excitatory postsynaptic potentials (EPSPS) were recorded in the stratum radiatum of the CA1 region by using glass microelectrodes filled with 3 M NaCl. fEPSPs or EPSPs were elicited at 0.1 Hz by a digital stimulator that fed by a stimulation isolator unit. All data analyses were performed with custom-written software in Igor Pro 8 (Wavemetrics). fEPSP or EPSP slope was measured as an index of synaptic strength. For whole-cell recordings, access resistance was monitored throughout the recording and only experiments with stable resistance were kept (changes<20%) and recordings were made from CA1 pyramidal neurons,

electrodes were filled with a solution containing the following (in mM): 120 K-gluconate, 20 KCl, 10 HEPES, 2 MgCl26H2O, and 2 Na2ATP.

Immunohistochemistry

Hippocampal slices of 100 μm were obtained from P30 to P40 old L15S or L15 mice. The slices were incubated in ACSF at RT for 1 h for recovery and fixed in 0.1 M Phosphate buffer (PB) containing 4% PFA, pH 7.4, overnight at 4°C. After fixation, slices were washed in 0.1 M PB and blocked with 1.5% heat-inactivated horse serum overnight at 4°C. Slices were incubated with primary anti-GLUA1 antibody (1:200, Alomone Lab, CAT# AGC-004) and primary anti-GLUA2 antibody (1:200, Alomone Lab, CAT# AGC-005) in blocking solution for 5 days at 4°C, washed with PB, and incubated with anti-rabbit secondary antibody conjugated to DyLight 649 (1:500; Jackson ImmunoResearch Laboratories) overnight. They are then washed and mounted with DAKO Fluorescent Mounting medium (Dako Canada) onto microscope slides before imaging and subsequent blinded analysis. Spine images were taken in z stacks using a Leica Microsystems SP8 confocal microscope with oil-immersion 63x objective at 6x zoom-in. The images were deconvolved and analyzed using software Huygens (Scientific Volume Imaging) and Imaris (Oxford Instruments) respectively. The experimenter was blinded to the treatment.

Immunoblotting

Hippocampi of WT and SPKO mice at P20 were obtained and rapidly homogenized in ice-cold RIPA (150 mM NaCl, 1% Nonidet P-40, 0.5% sodium deoxycholate,

0.1% sodium dodecylsulfate, 50 mM Tris-HCl (pH 8.0) with protease and phosphatase inhibitors (1X Roche Complete Mini, 5 mM NaF, 1 mM sodium orthovandate, 1 mM PMSF). Homogenates were sonicated and centrifuged for 5 min at 13,200 rpm. The supernatant was extracted and mixed with 2x Laemmli sample buffer to produce loading samples. Samples were boiled, resolved on SDS-PAGE, transferred to nitrocellulose, and stained with primary antibodies overnight. The following primary antibodies were used: GluA1 (1:1000, Abcam, ab31232), GluA2 (1:1000, Abcam, ab20673), GluN2A (1:1800, Abcam, ab124913,), GluN2B (1:1800, Abcam, ab65783), IP3R (1:1000, Cell Signaling, D53A5). Horseradish peroxidase (HRP)-conjugated secondary antibodies goat anti-rabbit (abcam; 1:5000) or goat anti-mouse (Bio-Rad Laboratories; 1:10,000) were applied for 1 h. The blots were imaged with Amersham Imager 600 and the band intensities were analyzed using the open-source program Fiji.

Acknowledgments and funding sources

This work was supported by National Institute of Mental Health R01MH108614 to A.F.; Canadian Institutes of Health Research MOP 86724 to R.A.M.; NSERC Discovery RGPIN-2020-06373 to R.A.M. and the Norman Zavalkoff Family Foundation to R.A.M.; Richard and Edith Strauss Postdoctoral Fellowship in Medicine to Y.I.; NSERC-USRA to J.T-K. We thank members of R.A.M. laboratories for comments on the manuscript; and Francois Charron for excellent technical assistance. The authors declare no competing financial interests.

Author contributions:

Y.I. and R.A.M. designed research; Y.I., P.Y.W, C.L.D and J.T-K. performed research; Y.I., P.Y.W., C.L.D. and J.T-K. analyzed data; Y.I., P.Y.W and R.A.M. wrote the paper.

References

1. Mundel, P., Heid, H.W., Mundel, T.M., Krüger, M., Reiser, J., and Kriz, W. (1997). Synaptopodin: An Actin-associated Protein in Telencephalic Dendrites and Renal Podocytes. J. Cell Biol. *139*, 193–204. 10.1083/jcb.139.1.193.

2. Verbich, D., Becker, D., Vlachos, A., Mundel, P., Deller, T., and McKinney, R.A. (2016). Rewiring neuronal microcircuits of the brain via spine head protrusions--a role for synaptopodin and intracellular calcium stores. Acta Neuropathol. Commun. *4*, 38. 10.1186/s40478-016-0311-x.

3. Vlachos, A., Ikenberg, B., Lenz, M., Becker, D., Reifenberg, K., Bas-Orth, C., and Deller, T. (2013). Synaptopodin regulates denervation-induced homeostatic synaptic plasticity. Proc. Natl. Acad. Sci. U. S. A. *110*, 8242–8247. 10.1073/pnas.1213677110.

4. Jedlicka, P., Vlachos, A., Schwarzacher, S.W., and Deller, T. (2008). A role for the spine apparatus in LTP and spatial learning. Behav. Brain Res. *192*, 12–19. 10.1016/j.bbr.2008.02.033.

5. Speranza, L., Inglebert, Y., De Sanctis, C., Wu, P.Y., Kalinowska, M., McKinney, R.A., and Francesconi, A. (2022). Stabilization of Spine Synaptopodin by mGluR1 Is Required for mGluR-LTD. J. Neurosci. *42*, 1666–1678. 10.1523/JNEUROSCI.1466-21.2022.

6. Wu, P.Y., Ji, L., De Sanctis, C., Francesconi, A., Inglebert, Y., and McKinney, R.A. (2023). Loss of synaptopodin impairs mGluR5 and protein synthesis dependent mGluR-LTD at CA3-CA1 synapses (Neuroscience) 10.1101/2023.08.02.551676.

7. Dudek, S.M., and Bear, M.F. (1992). Homosynaptic long-term depression in area CA1 of hippocampus and effects of N-methyl-D-aspartate receptor blockade. Proc. Natl. Acad. Sci. *89*, 4363–4367. 10.1073/pnas.89.10.4363.

8. Malenka, R.C., and Bear, M.F. (2004). LTP and LTD. Neuron *44*, 5–21. 10.1016/j.neuron.2004.09.012.

9. Holbro, N., Grunditz, Å., and Oertner, T.G. (2009). Differential distribution of endoplasmic reticulum controls metabotropic signaling and plasticity at hippocampal synapses. Proc. Natl. Acad. Sci. *106*, 15055–15060. 10.1073/pnas.0905110106.

10. Zhang, X. -l., Poschel, B., Faul, C., Upreti, C., Stanton, P.K., and Mundel, P. (2013). Essential Role for Synaptopodin in Dendritic Spine Plasticity of the Developing Hippocampus. J. Neurosci. *33*, 12510–12518. 10.1523/JNEUROSCI.2983-12.2013.

11. Dan, Y., and Poo, M.-M. (2006). Spike Timing-Dependent Plasticity: From Synapse to Perception. Physiol. Rev. *86*, 1033–1048. 10.1152/physrev.00030.2005.

12. Bi, G., and Poo, M. (1998). Synaptic modifications in cultured hippocampal neurons: dependence on spike timing, synaptic strength, and postsynaptic cell type. J. Neurosci. *18*, 10464–10472.

13. Debanne, D., Gähwiler, B.H., and Thompson, S.M. (1998). Long-term synaptic plasticity between pairs of individual CA3 pyramidal cells in rat hippocampal slice cultures. J. Physiol. *507*, 237–247.

14. Debanne, D., Gähwiler, B.H., and Thompson, S.M. (1996). Cooperative interactions in the induction of long-term potentiation and depression of synaptic excitation between hippocampal CA3-CA1 cell pairs in vitro. Proc. Natl. Acad. Sci. U. S. A. *93*, 11225–11230.

15. Debanne, D., Guérineau, N.C., Gähwiler, B.H., and Thompson, S.M. (1996). Paired-pulse facilitation and depression at unitary synapses in rat hippocampus: quantal fluctuation affects subsequent release. J. Physiol. *491*, 163–176. 10.1113/jphysiol.1996.sp021204.

16. Markram, H., Lübke, J., Frotscher, M., and Sakmann, B. (1997). Regulation of Synaptic Efficacy by Coincidence of Postsynaptic APs and EPSPs. Science *275*, 213–215. 10.1126/science.275.5297.213.

17. Andrade-Talavera, Y., Duque-Feria, P., Paulsen, O., and Rodríguez-Moreno, A. (2016). Presynaptic Spike Timing-Dependent Long-Term Depression in the Mouse Hippocampus. Cereb. Cortex N. Y. N 1991 *26*, 3637–3654. 10.1093/cercor/bhw172.

18. Inglebert, Y., and Debanne, D. (2021). Calcium and Spike Timing-Dependent Plasticity. Front. Cell. Neurosci. *15*, 727336. 10.3389/fncel.2021.727336.

19. Debanne, D., and Inglebert, Y. (2023). Spike timing-dependent plasticity and memory. Curr. Opin. Neurobiol. *80*, 102707. 10.1016/j.conb.2023.102707.

20. Feldman, D.E. (2012). The Spike-Timing Dependence of Plasticity. Neuron *75*, 556–571. 10.1016/j.neuron.2012.08.001.

21. Inglebert, Y., Aljadeff, J., Brunel, N., and Debanne, D. (2020). Synaptic plasticity rules with physiological calcium levels. Proc. Natl. Acad. Sci. U. S. A. *117*, 33639–33648. 10.1073/pnas.2013663117.

22. Wittenberg, G.M. (2006). Malleability of Spike-Timing-Dependent Plasticity at the CA3-CA1 Synapse. J. Neurosci. *26*, 6610–6617. 10.1523/JNEUROSCI.5388-05.2006.

23. Henley, J.M., and Wilkinson, K.A. (2016). Synaptic AMPA receptor composition in development, plasticity and disease. Nat. Rev. Neurosci. *17*, 337–350. 10.1038/nrn.2016.37.

24. Paoletti, P., Bellone, C., and Zhou, Q. (2013). NMDA receptor subunit diversity: impact on receptor properties, synaptic plasticity and disease. Nat. Rev. Neurosci. *14*, 383–400. 10.1038/nrn3504.

25. Mockett, B., Coussens, C., and Abraham, W.C. (2002). NMDA receptor-mediated metaplasticity during the induction of long-term depression by low-frequency stimulation: Priming of LTD during low frequency stimulation. Eur. J. Neurosci. *15*, 1819–1826. 10.1046/j.1460-9568.2002.02008.x.

26. Forsberg, M., Seth, H., Björefeldt, A., Lyckenvik, T., Andersson, M., Wasling, P., Zetterberg, H., and Hanse, E. (2019). Ionized calcium in human cerebrospinal fluid and its influence on intrinsic and synaptic excitability of hippocampal pyramidal neurons in the rat. J. Neurochem. *149*, 452–470. 10.1111/jnc.14693.

27. Jedlicka, P., Schwarzacher, S.W., Winkels, R., Kienzler, F., Frotscher, M., Bramham, C.R., Schultz, C., Bas Orth, C., and Deller, T. (2009). Impairment of in vivo theta-burst long-term potentiation and network excitability in the dentate gyrus of synaptopodin-deficient mice lacking the spine apparatus and the cisternal organelle. Hippocampus *19*, 130–140. 10.1002/hipo.20489.

28. Aloni, E., Verbitsky, S., Kushnireva, L., Korkotian, E., and Segal, M. (2021). Increased excitability of hippocampal neurons in mature synaptopodin-knockout mice. Brain Struct. Funct. *226*, 2459–2466. 10.1007/s00429-021-02346-0.

29. Lee, H.-K., and Kirkwood, A. (2019). Mechanisms of Homeostatic Synaptic Plasticity in vivo. Front. Cell. Neurosci. *13*, 520. 10.3389/fncel.2019.00520.

30. Dubes, S., Soula, A., Benquet, S., Tessier, B., Poujol, C., Favereaux, A., Thoumine, O., and Letellier, M. (2022). miR-124-dependent tagging of synapses by synaptopodin enables input-specific homeostatic plasticity. EMBO J. *41*, e109012. 10.15252/embj.2021109012.

31. Nevian, T., and Sakmann, B. (2006). Spine Ca2+ Signaling in Spike-Timing-Dependent Plasticity. J. Neurosci. *26*, 11001–11013. 10.1523/JNEUROSCI.1749-06.2006.

32. Yang, S.-N., Tang, Y.-G., and Zucker, R.S. (1999). Selective Induction of LTP and LTD by Postsynaptic $[Ca^{2+}]_i$ Elevation. J. Neurophysiol. *81*, 781–787. 10.1152/jn.1999.81.2.781.

33. Lisman, J. (1989). A mechanism for the Hebb and the anti-Hebb processes underlying learning and memory. Proc. Natl. Acad. Sci. *86*, 9574–9578. 10.1073/pnas.86.23.9574.

34. Korkotian, E., and Segal, M. (2011). Synaptopodin regulates release of calcium from stores in dendritic spines of cultured hippocampal neurons: Synaptopodin regulates calcium release. J. Physiol. *589*, 5987–5995. 10.1113/jphysiol.2011.217315.

35. Fuenzalida, M., Fernández de Sevilla, D., Couve, A., and Buño, W. (2010). Role of AMPA and NMDA receptors and back-propagating action potentials in spike timing-dependent plasticity. J. Neurophysiol. *103*, 47–54. 10.1152/jn.00416.2009.

36. Holbro, N., Grunditz, A., Wiegert, J.S., and Oertner, T.G. (2010). AMPA receptors gate spine Ca(2+) transients and spike-timing-dependent potentiation. Proc. Natl. Acad. Sci. U. S. A. *107*, 15975–15980. 10.1073/pnas.1004562107.

Figure legends

Figure1. SPKO mice show a deficit of LFS-LTD and HFS-LTP. (A) Diagram showing the positions of stimulating and recording electrodes at the Sc-CA1 synapses. **(B)** BCM curves in WT and SPKO for 2, 10 and 100 Hz stimulation frequency. **(C)** *(Left)* Time course of normalized fEPSP in WT and SPKO following 2Hz (900 pulses) stimulation. *(Right)* Quantification of average synaptic modification in the last 10 minutes of the recording. **(D)** *(Left)* Time course of normalized fEPSP in WT and SPKO following 10Hz (900 pulses) stimulation. *(Right)* Quantification of average synaptic modification in the last 10 minutes of the recording. **(E)** *(Left)* Time course of normalized fEPSP in WT and SPKO following 100Hz (900 pulses) stimulation. *(Right)* Quantification of average synaptic modification in the last 10 minutes of the recording.

Figure 2. Spike-Timing Dependent Plasticity is altered in SPKO. (A) *(Left)* Diagram showing the positions of stimulating electrodes and recording electrodes at the Sc-CA1 synapses. *(Right)* Illustration of the pre-before-post (100p@0.3Hz) and post-before-pre (100p@0.3Hz) protocol used to induce synaptic modification. **(B)**. *(Left)* Time course of normalized EPSP in WT and SPKO following pre-before-post protocol at +10ms. *(Right)*. Quantification of average synaptic modification (*closed circles*) in the last 10 minutes of the recording with individuals' values for each cell (*open circles*). **(C)**. STDP curves in WT and SPKO for pre-before-post protocol at different timings. **(D)**. *(Left)* Time course of normalized EPSP in WT and SPKO following post-before-pre protocol at -25ms. *(Right)*. Quantification of average synaptic modification (*closed circles*) in the last 10 minutes of the recording with individuals' values for each cell (*open circles*).

Figure 3. t-LTP but not t-LTD can be restored in SPKO. (A). *(Left)* Time course of normalized EPSP in WT and SPKO following pre-before-post (+10ms) protocol at 0.3 or 5 Hz. *(Right)*. Quantification of average synaptic modification (*closed circles*) in the last 10 minutes of the recording with individuals' values for each cell (*open circles*). **(B).** *(Left)* Time course of normalized EPSP in WT and SPKO following post-before-pre (-25ms) protocol at 0.3, 5 or 10 Hz. *(Right)*. Quantification of average synaptic modification (*closed circles*) in the last 10 minutes of the recording with individuals' values for each cell (*open circles*).

Figure 4. GluA1, GluA2 and IP3R are decreased in SPKO. (A). Representative immunoblot and quantification of total (*left*) GluA1 and (*right*) GluA2 from hippocampi of WT (n=5) and SPKO (n=5) mice. **(B) (C).** Representative images

and quantification of CA1 pyramidal neuron tertiary dendrites immunostained with surface GluA1 antibody (WT n=12, KO n=14) and surface GluA2 antibody (WT n=13, KO n=11) in acute hippocampal slices. Scale bar=3 μm. **(D).** Representative immunoblot and quantification of total (left) NR2A and (right) NR2B from hippocampi of WT (n=5) and SPKO (n=5) mice. **(E).** Representative immunoblot and quantification of total IP3R from hippocampi of WT (n=8) and SPKO (n=8) mice.

Figure 1

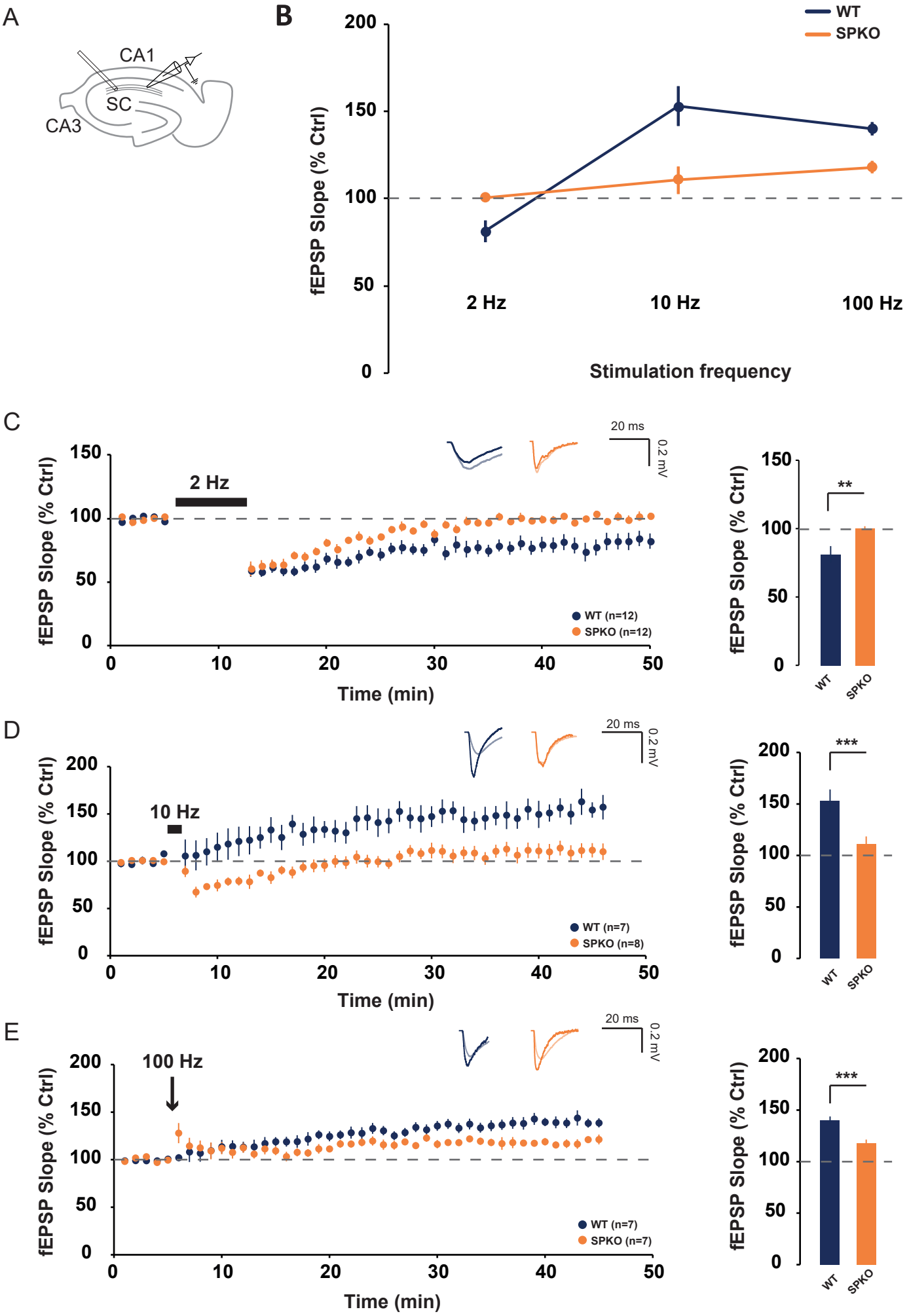
A
CA1
SC
CA3
B
WT
SPKO
fEPSP Slope (% Ctrl)
200
150
100
50
0
2 Hz
10 Hz
100 Hz
Stimulation frequency
C
20 ms
0.2 mV
2 Hz
WT (n=12)
SPKO (n=12)
Time (min)
**
WT
SPKO
D
10 Hz
WT (n=7)
SPKO (n=8)
***
E
100 Hz
WT (n=7)
SPKO (n=7)

Figure 2

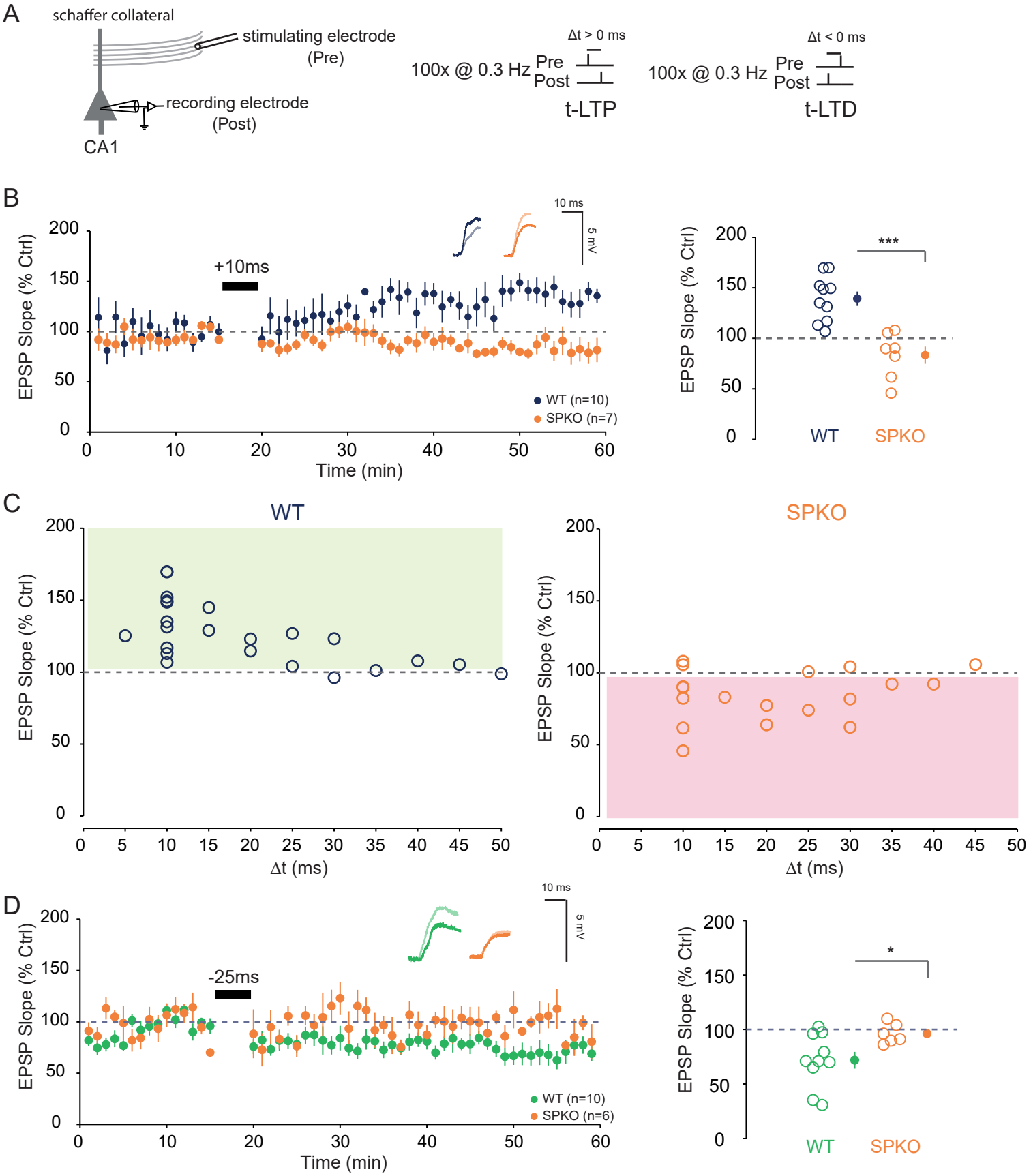
A
schaffer collateral
stimulating electrode
(Pre)
recording electrode
(Post)
CA1
100x @ 0.3 Hz
Pre
Post
Δt > 0 ms
t-LTP
100x @ 0.3 Hz
Pre
Post
Δt < 0 ms
t-LTD
B
EPSP Slope (% Ctrl)
+10ms
10 ms
5 mV
WT (n=10)
SPKO (n=7)
Time (min)
***
WT
SPKO
C
WT
SPKO
EPSP Slope (% Ctrl)
Δt (ms)
D
EPSP Slope (% Ctrl)
-25ms
10 ms
5 mV
WT (n=10)
SPKO (n=6)
Time (min)
*
WT
SPKO

Figure 3

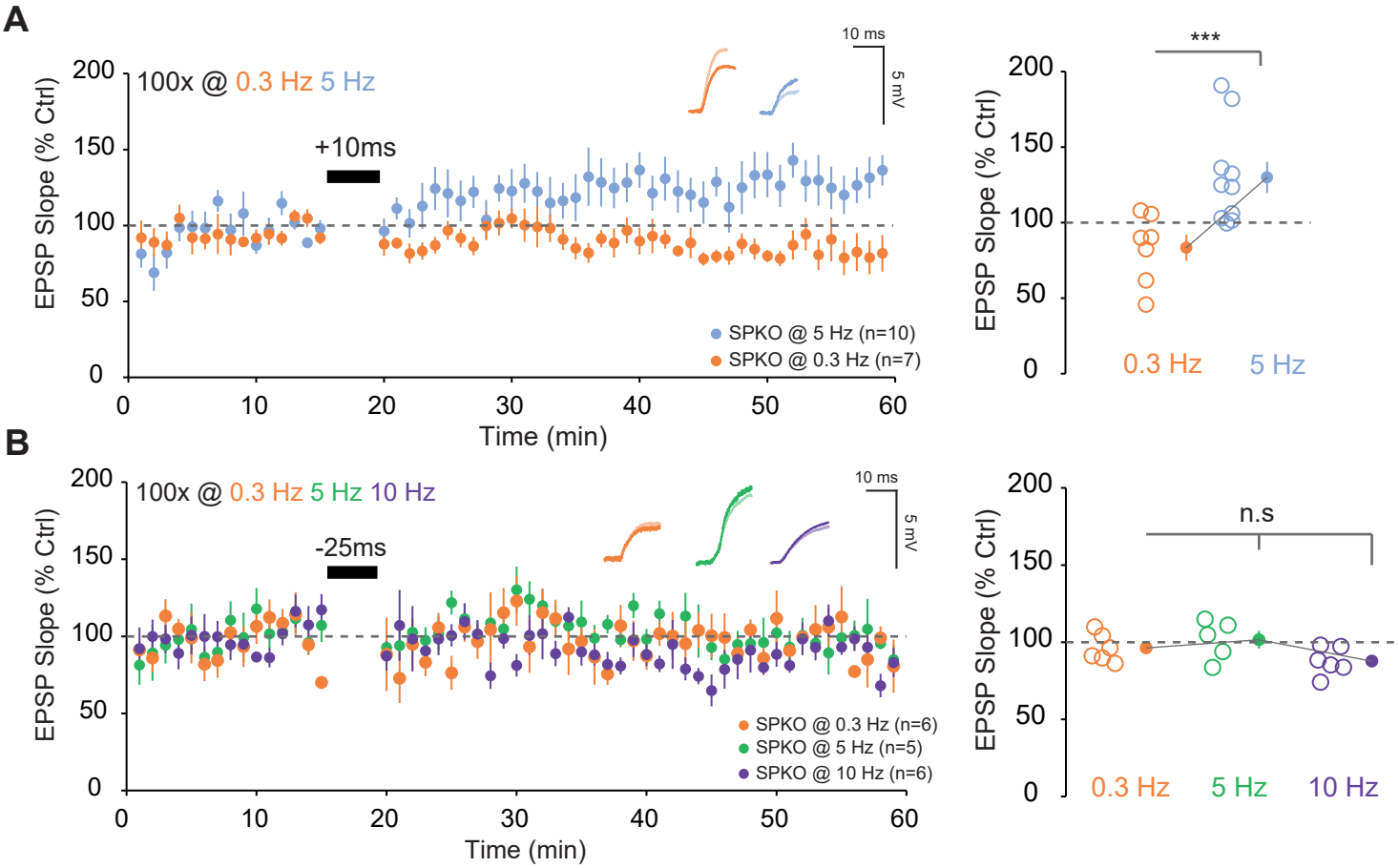
A
100x @ 0.3 Hz 5 Hz
+10ms
10 ms
5 mV
EPSP Slope (% Ctrl)
Time (min)
SPKO @ 5 Hz (n=10)
SPKO @ 0.3 Hz (n=7)
***
0.3 Hz
5 Hz
B
100x @ 0.3 Hz 5 Hz 10 Hz
-25ms
SPKO @ 0.3 Hz (n=6)
SPKO @ 5 Hz (n=5)
SPKO @ 10 Hz (n=6)
n.s
0.3 Hz
5 Hz
10 Hz

Figure 4

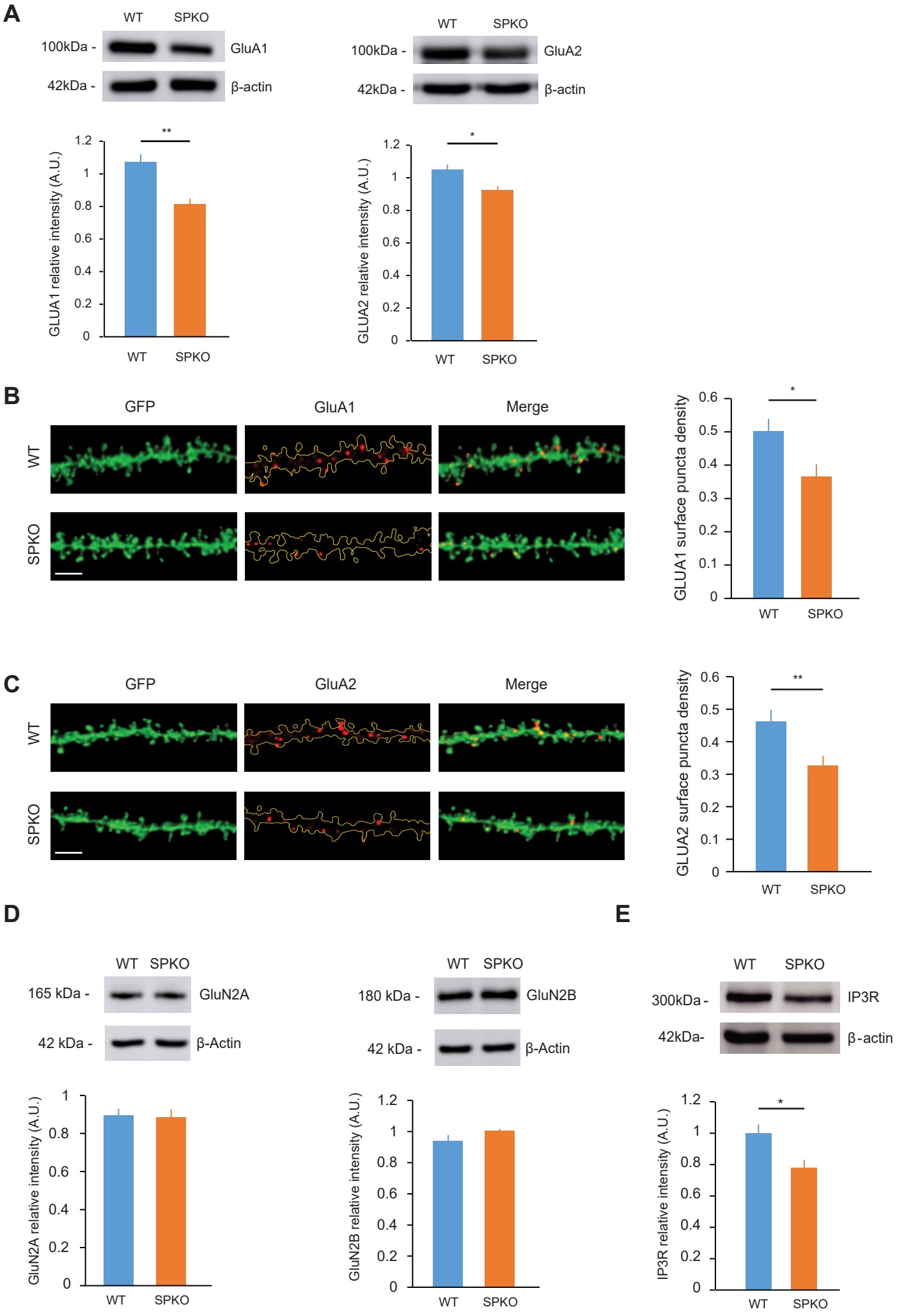
A
WT
SPKO
100kDa -
GluA1
42kDa -
β-actin
GLUA1 relative intensity (A.U.)
**
WT
SPKO
100kDa -
GluA2
42kDa -
β-actin
GLUA2 relative intensity (A.U.)
*
B
GFP
GluA1
Merge
WT
SPKO
GLUA1 surface puncta density
*
C
GFP
GluA2
Merge
GLUA2 surface puncta density
**
D
165 kDa -
GluN2A
42 kDa -
β-Actin
GluN2A relative intensity (A.U.)
180 kDa -
GluN2B
GluN2B relative intensity (A.U.)
E
300kDa -
IP3R
42kDa-
IP3R relative intensity (A.U.)